



## Research paper

# Study on the temperature field and deformation of ultra-high hollow thin-walled piers under solar radiation

Xiangyu Hou<sup>1</sup>, Haibing Wu<sup>2</sup>, Shiliang Zhang<sup>3</sup>,  
Da Ma<sup>4</sup>, Chaojie Miao<sup>5</sup>, Jun Hu<sup>6</sup>

**Abstract:** To analyse the solar temperature field and deformation of ultra-high hollow thin-walled piers, based on the 192 m thin-walled hollow piers of Lugou River Bridge in Chongqing, China, the two most unfavourable temperature fields of high temperature in summer and low temperature in winter are selected. The variation rule of wall temperature and displacement of piers under the action of solar radiation is studied using finite element software ANSYS, and the influence of cross-sectional changes of piers on the displacement of pier tops is analysed in detail. The results indicate that the finite element solution in this paper is in good agreement with the literature solution, which verifies the reliability of the finite element analysis in this paper. The temperature change of the east and west pier walls is the most significant in the high temperature environment in summer, and the temperature change of the south pier wall is more obvious in the low temperature environment in winter. The deformation of the pier in winter is significantly greater than that in summer under the action of sunlight. When the volume of the pier remains unchanged, the displacement of the octagonal section pier is close to that of the rectangular section pier. Due to the increase in cross-sectional stiffness, the round-end pier can effectively reduce the displacement of the pier body caused by sunlight.

**Keywords:** parameter analysis, solar radiation, temperature effects, ultra-high hollow thin-walled piers

<sup>1</sup>Eng., Board of Supervisors, Chongqing Yuxiang Double Track Expressway Co., Ltd., Chongqing, 408599, China, e-mail: [houxiangyu@cegc.com.cn](mailto:houxiangyu@cegc.com.cn), ORCID: 0009-0003-0290-234X

<sup>2</sup>Eng., Chief Engineer Office of, Yuxiang Project, China State Construction Railway Investment and Engineering Group Co., Ltd., Beijing, 102628, China, e-mail: [250236692@qq.com](mailto:250236692@qq.com), ORCID: 0009-0001-6436-1468

<sup>3</sup>Eng., Engineering Management Department, China State Construction Railway Investment and Engineering Group Co., Ltd., Beijing, 102628, China, e-mail: [867554695@qq.com](mailto:867554695@qq.com), ORCID: 0009-0009-6941-0060

<sup>4</sup>Eng., Engineering Management Department, Chongqing Yuxiang Double Track Expressway Co., Ltd., Chongqing, 408599, China, e-mail: [563547353@qq.com](mailto:563547353@qq.com), ORCID: 0009-0002-5525-801X

<sup>5</sup>Eng., Technical Contracts Department, Chongqing Yuxiang Double Track Expressway Co., Ltd., Chongqing, 408599, China, e-mail: [874098896@qq.com](mailto:874098896@qq.com), ORCID: 0009-0000-0201-1561

<sup>6</sup>Prof., PhD., School of Civil Engineering, Chongqing Jiaotong University, Chongqing, 400074, China, e-mail: [hujun@cqjtu.edu.cn](mailto:hujun@cqjtu.edu.cn), ORCID: 0000-0003-1165-0458

## 1. Introduction

With the rapid development of China's transportation construction, highways and railways gradually extend to the southwest of mountains, valleys, and ravines. Continuous rigid bridges with ultra-high piers are widely used due to their strong spanning capacity and economy. Under the action of sunshine and air temperature, the sunny and shady sides of the hollow thin-walled piers will produce a large temperature difference, while the ultra-high piers have a large slenderness ratio, and the stiffness of the pier top is poor when it is unconstrained, which makes the pier deform significantly in the horizontal plane and has an important impact on the verticality control of the pier [1, 2]. Therefore, it is necessary to study the solar temperature field and deformation of ultra-high hollow thin-walled piers.

The intensity of solar radiation can significantly affect the inhomogeneity of the temperature field of the structure [3]. Chen *et al.* [4] conducted a long-term test for the non-uniform temperature field of the cross-section of the hollow thin-walled pier and found that the influence depth under the mixed action of air temperature and sunshine did not exceed 50 cm. The sunshine radiation intensity was the controlling factor for the most unfavorable positive temperature difference. According to the observed temperature field, the temperature difference distribution curve in the form of a power function with high accuracy is fitted. Dai *et al.* [5, 6] pointed out the main influencing factors of bridge temperature field, and proposed a more accurate prediction model of pier extreme temperature based on long-term test data. An *et al.* [7] used the analytical method to obtain the calculation formula for the displacement of hollow thin-walled piers under the sunlight. Mi *et al.* [8] proposed a set of algorithms suitable for the horizontal displacement of piers with complex cross-section forms under arbitrary temperature fields, which has an error of less than 5% from the simulated value. In addition, the temperature field of the pier under sudden cooling was also studied [9, 10].

Many scholars have studied the influencing factors of the temperature field of the structure. Wang *et al.* [11] found that the surface position of the pier and the total amount of sunlight absorbed were the most significant factors affecting the temperature stress. Gao *et al.* [12] used a temperature sensor to monitor the temperature distribution of the pier during a certain maintenance period, and found that the atmospheric fluctuation had a significant effect on the temperature of the outer surface of the pier. Hu *et al.* [13] considered the shading effect of the surrounding mountains and beam superstructure on the piers, and established the calculation formula for the shadow parts on the surface of the piers, and obtained the necessary conditions for the pier wall to receive sunlight. Yuan *et al.* [14] analyzed the temperature and displacement of the piers before and after applying the reflective thermal insulation coating by finite element software. Fu [15] analyzed the thermal conductivity and atmospheric transparency that greatly influenced the temperature field of the pier and gave the variation rule of the temperature field.

Determining the amount of solar radiation on the surface of the structure is of great significance for the temperature field analysis of the structure under the action of sunlight [16]. Wang [17] used the finite element software ANSYS to study the sunshine temperature effect of concrete hollow thin-walled piers, and gave the calculation methods of solar radiation, convective heat transfer and long-wave radiation heat transfer on the surface of the piers. Mao [18] gave a method for calculating the temperature field of piers under solar radiation, and

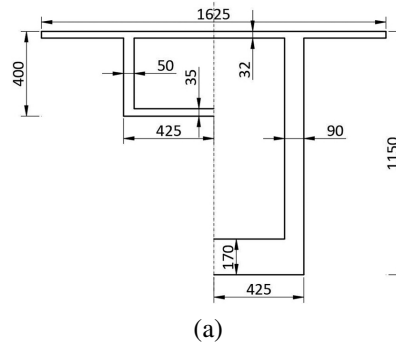
developed a general software for calculating the temperature field of the structure using the C++ language. Combined with the temperature observation test of concrete slab, the reliability of the software was verified, and then the temperature field and pier deformation of the hollow high pier were analyzed by using ANSYS. In summary, the existing research literature on the temperature of hollow piers pays more attention to the influence of temperature stress and displacement. It rarely involves the influence of the change of the pier parameters on the temperature and deformation of the pier.

In this paper, the ultra-high hollow thin-walled pier model is established by using the finite element software ANSYS to obtain the temperature distribution and displacement of the thin-walled pier under the most unfavorable sunlight. By solving the engineering example, the influence of the change of the pier's cross-section form on the pier's deformation is analyzed in detail.

## 2. Engineering background

Located in Chaoyang Village, Dongquan Town, Banan District, Chongqing, China, the Lugou River Bridge spans the Lugou River, about 7.2 km from Dongquan Town. The bridge is detached, the left bridge starts and ends with the stations ZK27+661~ZK29+809, the bridge length is 2148 m, and the hole span is  $3 \times 40 + (96 + 5 \times 180 + 96) + 23 \times 40$  m for the left line bridge. The start and end stations of the right line bridge are K27+606~K29+794, the bridge length is 2188 m, and the hole span is  $4 \times 40 + (96 + 5 \times 180 + 96) + 23 \times 40$  m. The width of the bridge deck on the left and right lines is 16.25 m, and the maximum pier height is 192 m, which is the No. 7 pier on the left. The longitudinal slopes of the left and right lines are 1.95% and 2.85% respectively.

The bridge adopts a single box and a single chamber, with a top width of 16.25 m, a bottom width of 8.5 m, a unilateral cantilever length of 3.875 m, a height of 4 m in the middle of the box girder, a height of 11.5 m at the root, and a parabolic change in 1.5 times in the beam height and bottom plate thickness. The box girder web adopts three levels of 0.5 m, 0.7 m and 0.9 m. The mid-span and root cross-sections and outer contours of the bridge are shown in Fig. 1.



In this paper, the temperature field analysis is carried out based on the No. 7 hollow thin-walled pier of the Lugou River Bridge. The longitude of the bridge site is  $106.8^\circ$  and the latitude is  $29.4^\circ$ . The height of the pier is 192 m, and the wall thickness of the pier body gradually

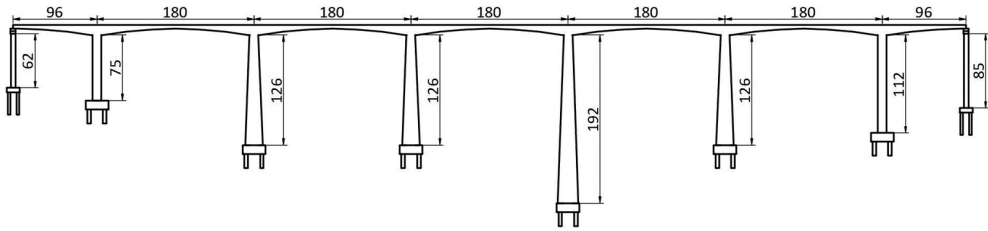


Fig. 1. Schematic diagram of the bridge cross-section and elevation: (a) Schematic diagram of the bridge cross-section (unit: cm), (b) Schematic diagram of the bridge elevation (unit: m)

changes from 1.4 m at the bottom of the pier to 0.8 m at the top of the pier. The transverse size at the bottom of the pier is 16.4 m, the size along the bridge is 14.9 m, and it narrows to the top of the pier according to the slope ratio of 60:1. The size of the cap is 21 m × 21 m × 7 m. The pier body section and the orientation of each wall surface are shown in Fig. 2.

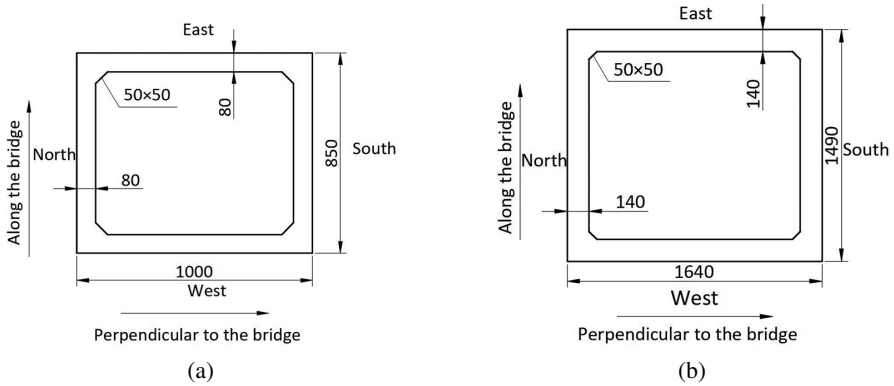


Fig. 2. Schematic diagram of the pier cross-section (unit: cm): (a) The pier top cross-section, (b) The pier bottom cross-section

### 3. Analysis method and verification of the pier temperature field

#### 3.1. Theoretical analysis of the temperature field

##### 3.1.1. Heat exchange way

There are three main ways of heat exchange between concrete hollow thin-walled piers and the external environment [17], namely

##### 1. Sunlight shortwave radiation

Sunlight radiation comprises direct sunlight radiation intensity and sunlight diffuse radiation intensity. When sunlight radiation passes through the atmosphere and reaches

the ground, the heat flux density  $q_s$  of sunshine shortwave radiation on the surface of the pier is

$$(3.1) \quad q_s = [I_d \cos \phi + I_{dH}(1 + \sin \beta_n)/2 + (I_d \sin \beta_s + I_{dH})(1 - \sin \beta_n)r/2]A_s$$

where:  $I_d$  – the intensity of solar radiation reaching the ground,  $[W/m^2]$ ,  $I_{dH}$  – the intensity of solar scattering,  $[W/m^2]$ ,  $\phi$  – the sun incidence angle,  $[^\circ]$ ,  $\beta_n$  – the angle between the normal of the object surface and the horizon,  $[^\circ]$ ,  $\beta_s$  – the angle of the solar altitude,  $[^\circ]$ ,  $r$  – the surface shortwave emissivity,  $A_s$  – the absorption rate of shortwave radiation.

## 2. Long-wave radiative heat transfer

Long-wave radiative heat transfer is the process of heat transfer between the pier surface and the external environment through radiation, wherein the long-wave radiant heat flux density  $q_r$  absorbed by the pier surface is

$$(3.2) \quad q_r = \varepsilon C_0 [(273 + T_a)^4 - (273 + T)^4] - \varepsilon C_0 (273 + T_a)^4 (1 - \varepsilon_a)(1 + \sin \beta_n)/2$$

where:  $\varepsilon$  – the long-wave emissivity of the pier surface,  $C_0$  – the Stephen-Boltzmann constant,  $[W/(m^2 \cdot K^4)]$ ,  $T_a$  – the atmospheric temperature,  $[^\circ C]$ ,  $T$  – the surface temperature of the pier,  $[^\circ C]$ ,  $\varepsilon_a$  – the atmospheric emissivity.

## 3. Convection heat transfer

Convective heat transfer is the process of heat transfer between the atmosphere and the pier surface through airflow, wherein the convective heat transfer heat flux density  $q_c$  flowing into the pier surface is

$$(3.3) \quad q_c = h_c(T_a - T)$$

where:  $h_c$  – the convective heat transfer coefficient,  $[W/(m^2 \cdot K)]$ .

### 3.1.2. Boundary conditions

After obtaining the heat flux density, the distribution of the temperature field of the pier can be calculated by the initial conditions and the temperature boundary conditions. For the temperature field, there are three commonly used boundary conditions. The third type of boundary condition is used in this paper, that is, the convective heat transfer relationship of the pier surface is known with time. Converting the above heat flux to the third type of boundary condition, the total heat flux density  $q$  can be expressed as

$$(3.4) \quad q = q_s + q_r + q_c = h(T_a^* - T)$$

where:  $h$  – the comprehensive heat exchange coefficient,  $[W/(m^2 \cdot K)]$ ,  $T_a^*$  – the comprehensive air temperature,  $[^\circ C]$ .

## 3.2. Modeling and analysis method of the pier temperature field

The basic principle of finite element analysis of the pier temperature field is to divide the pier into several elements that intersect at the node and obtain the temperature at the node by solving the thermal differential equation of the node under certain initial conditions and boundary conditions.

### 3.2.1. Description of the finite element model

When analyzing the temperature field of the pier, the finite element modeling is performed using a 3-dimensional 8-node SOLID278 element in ANSYS, where the degree of freedom is temperature. The pier temperature is analyzed in a transient manner, the time step is set to one hour, and multiple load steps are applied using loop statements and arrays. After the transient thermal analysis, the general post-processor is used to view the node temperature, and the time-history post-processor is used to view the temperature change rule with time. Once the pier temperature field has been analyzed, the temperature element SOLID278 can be converted into the corresponding structural element SOLID185 using the ETCHG command flow. Then, all temperature loads are deleted, the corresponding material properties and reference temperatures are set, and the cap node displacement is constrained. Finally, the LDREAD command flow is used to apply the temperature field as a load to the model to realize the static analysis.

### 3.2.2. Material parameters

In this paper, the density of the material used is  $2500 \text{ kg/m}^3$ , the specific heat capacity is  $880 \text{ J/(kg}\cdot\text{K)}$ , the thermal conductivity is  $2.5 \text{ W/(m}\cdot\text{K)}$ , the thermal expansion coefficient is  $1 \times 10^{-5} / ^\circ\text{C}$ , the elastic modulus is  $34.5 \text{ GPa}$ , and the Poisson's ratio is  $0.25$ . The solar radiation absorption rate of the concrete surface is  $0.65$  and the emissivity of longwave radiation is  $0.9$ .

### 3.2.3. Simulate operating conditions and load application

#### 1. Simulate operating conditions

Since the intensity of solar radiation varies with the ordinal number, to better simulate the deformation of the pier in practice, the two most unfavorable temperature fields of high temperature and high radiation in summer and low temperature and low radiation in winter were selected for the temperature effect analysis of the pier.

#### 2. Load application

There are three main ways of heat propagation: heat convection, heat conduction, and heat radiation. In the analysis of the temperature field of the pier, heat conduction occurs inside the concrete structure, and the heat is transferred from the high-temperature part to the low-temperature part. The thermal conductivity of the concrete determines its conduction speed, and only the thermal conductivity of the concrete material needs to be entered in the finite element analysis. For heat convection and heat radiation, the heat radiation heat flux density and convective heat exchange heat flux density can be obtained by substituting the geographical parameters, environmental parameters, azimuth angle and calculation date of the pier into Eqs. (3.1), (3.2) and (3.3), and the comprehensive air temperature and comprehensive heat exchange coefficient can be obtained by bringing them into Eq. (3.4). For thermal convection and thermal radiation, the application of thermal convection and thermal radiation load can be completed by applying the comprehensive air temperature and comprehensive heat transfer coefficient obtained by Eq. (3.4) to the surface of the pier in the form of convective heat transfer during finite element analysis.

### 3. Initial conditions

In the transient thermal analysis, it is necessary to determine the initial temperature state of the pier. The temperature of the pier one hour before sunrise can generally be selected, and the initial temperature field conditions can be obtained through cyclic iteration when the measured data is missing. In this paper, the second method is adopted. Firstly, the average air temperature of the day is set as the initial temperature of the finite element model of the pier, and the temperature field of the pier at different times is obtained by iterative calculation by considering solar radiation, heat convection, and heat conduction. In this model, 120 load steps are set for 5 days with 1 hour as the time step, and each load step includes 6 load sub-steps, and each load sub-step adopts the form of gradual load (i.e., linear load). When the pier temperature is calculated to the fifth day, the temperature field converges greatly, so the temperature field at this time is used as the initial condition for the analysis of the pier temperature field.

### 3.3. Model validation

In order to verify the correctness of the research method in this paper, the finite element software ANSYS was used to solve two numerical examples in the literature [18], and compared with the measured and calculated values.

Example 1: The concrete slab of  $2\text{ m} \times 2\text{ m} \times 1\text{ m}$  was placed horizontally for the test, and the temperature field was analyzed on August 9. The maximum temperature of the day was  $33.6^\circ\text{C}$ , the minimum temperature was  $21.2^\circ\text{C}$ , the longitude of the test site was  $117^\circ$ , the latitude was  $40^\circ$ , the altitude was  $33\text{ m}$ , and the azimuth angle was  $0^\circ$ . The density of concrete is  $2500\text{ kg/m}^3$ , the thermal conductivity is  $2.9\text{ W/(m}\cdot\text{K)}$ , and the specific heat capacity is  $950\text{ J/(kg}\cdot\text{K)}$ . The calculated temperature values of the internal and external measurement points of the concrete and the values obtained in the literature are shown in Table 1, and the measured values and calculated values are obtained by measuring the temperature curve graph.

Table 1. Comparison of temperature calculation results

Time (h)	Article value ( $^\circ\text{C}$ )		Measured value ( $^\circ\text{C}$ )		Literature value ( $^\circ\text{C}$ )	
	Surface measuring points	Internal measurement points	Surface measuring points	Internal measurement points	Surface measuring points	Internal measurement points
6	25.1	26.0	25.8	26.4	22.8	24.4
10	37.5	29.3	39.3	27.8	36.4	26
14	46.6	35.2	45.6	33.1	45.6	31.9
18	38.5	36.7	37.6	34.3	36.9	34.3
22	30.2	32.9	30.3	32.2	27.7	31.5

As can be seen from the table, except for a few time points, the temperature value in this paper is quite different from the measured value, and on the whole, the calculated value in this paper is in good agreement with the measured value.

Example 2: The longitude of the rectangular hollow thin-walled pier is  $103.3^\circ$ , the latitude is  $25^\circ$ , the altitude is 1736 m, and the pier height is 54.5 m. The length of pier wall 1 and 3 is 6.6 m and the thickness is 0.5 m, and the length of pier wall 2 and 4 is 3m and the thickness is 0.8 m, of which pier wall 1 is  $30^\circ$  south-west. Select January 15 as the calculation date. The elastic modulus is 32.5 GPa, the Poisson's ratio is 0.2, and the coefficient of thermal expansion is  $1.0 \times 10^{-5}/^\circ\text{C}$ . The maximum temperature on the day was  $21^\circ\text{C}$ , the minimum temperature was  $2^\circ\text{C}$ , and the average wind speed was set to 1m/s. The other parameters are the same as those in Example 1. The temperature of the pier wall on each side of the pier at different times is calculated as shown in Table 2. The maximum displacement of the pier crest under the most unfavorable temperature gradient is calculated as shown in Table 3.

Table 2. Comparison of temperature calculation results

Time (h)	Article value ( $^\circ\text{C}$ )				Literature value ( $^\circ\text{C}$ )			
	1	2	3	4	1	2	3	4
6	5.4	5.4	5.4	5.4	5.6	5.9	5.8	5.9
10	9.6	9.4	9.9	20.6	10.9	9.4	9.4	21.5
14	24.8	14.1	14.3	24.4	27	13.7	13.7	23.2
18	27.8	20.1	13.9	17.1	26.6	18.1	13	16.3

Table 3. Comparison of displacement calculation results

Direction	Article value (mm)	Literature value (mm)
Perpendicular to the bridge	2.7	3
Follow the bridge	28.6	31
Vertical	4.1	5
Displacement vectors	29	32

It can be seen from the table that the temperature obtained in this paper is close to the literature value, and the difference between the calculated temperature at each moment is not more than  $2.2^\circ\text{C}$ . The displacement errors are relatively small, which indicates that the model analysis effect in this paper is good and verifies the reliability of the research method.

## 4. Temperature and displacement analysis of the engineering pier

According to the actual size of the pier relying on the project, the finite element model of the pier is shown in Fig. 3. The model has a total of 27,840 elements and 33,648 nodes, and the influence of rebar is not considered in the analysis of this paper.

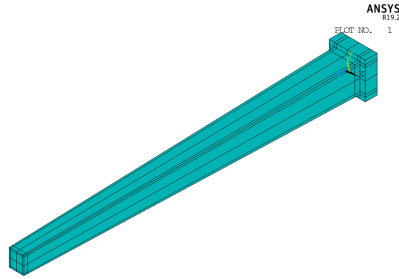


Fig. 3. Finite element model of the pier

#### 4.1. The pier temperature and displacement in summer

The highest temperature is  $36^{\circ}\text{C}$ , and the lowest is  $27^{\circ}\text{C}$ . The temperature change of the pier's outer surface in four directions was extracted and analyzed in a day. The temperature results are shown in Fig. 4. As can be seen from Fig. 4, at about 6 o'clock, the surface temperature of the pier begins to rise, and the east side is the most significant, which is because the sun rises, and the east side receives solar radiation first. At about 10 o'clock, the solar radiation moves to the east and south sides, and the temperature of the south side gradually increases. Near 11 o'clock, the temperature of the pier's east side appears to be at an extreme value. The size is  $45^{\circ}\text{C}$ , then it gradually decreases, and the temperature of the west side begins to rise. At 18 o'clock, the temperature of the west side rises to  $47^{\circ}\text{C}$ , which is nearly  $12^{\circ}\text{C}$  higher than the temperature of the other three sides. At 21 o'clock, the sun has set, and the temperature of each surface begins to drop. At 24 o'clock, the surface temperature of the pier continues to decrease through convection heat transfer under the condition that the external atmospheric temperature drops and the heat energy stored inside during the day is gradually lost. The internal temperature is gradually stabilized, reaching about  $30^{\circ}\text{C}$ .

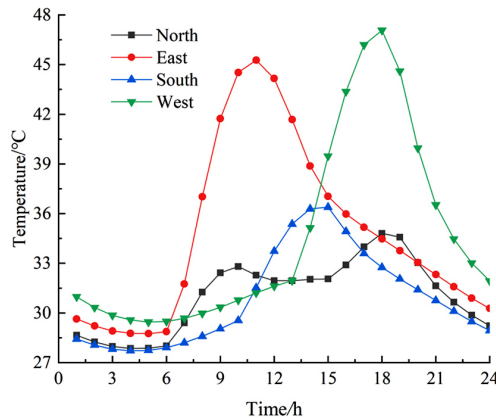


Fig. 4. Curve of pier temperature with time

In one day, the temperature change of the east and west pier walls was the most significant in the summer high temperature environment. The temperature change range of the east side was 18°C, and the temperature change range of the west side was 19°C.

To further illustrate the overall displacement of the pier, a horizontal section was taken at intervals of 50 m or 42 m in the height range of the pier from 0–192 m, and the displacement of each section was extracted and analyzed within one day. As shown in Fig. 5, with the increase in height, the pier's displacement becomes increasingly obvious. Before sunrise, the displacement curve of the pier in all directions is relatively gentle.

As can be seen from Fig. 5(a), the displacement of the pier body along the west gradually increases after sunrise, and the maximum value appears at 12 o'clock. Then, solar radiation acts on the south and west sides, and the temperature difference on the southwest side rises at this time. The temperature difference between the southwest and southeast sides decreases, so the pier displaces in the east direction. The pier displacement appears in the east direction at 19 o'clock. After sunset, the temperature of each pier wall slowly decreases and tends to be uniform.

As shown in Fig. 5(b), solar radiation acts on the north and east sides after sunrise, and the piers deform in the southerly direction, with a maximum at 10 o'clock. From 10 o'clock to 15 o'clock, the solar radiation acts on the west and south sides, the temperature of the south pier wall increases and the north side decreases, and the pier displaces in the north direction and appears to the maximum value at 15 o'clock. Subsequently, there was no radiation effect on the pier's south side, but the north side was displaced along the south direction due to radiation heating. After sunset, the pier displacement begins to recover slowly.

In one day, the maximum displacement of the pier top along the direction of the bridge is 26 mm. The displacement of the pier top in the direction perpendicular to the bridge is smaller than that along the direction of the bridge, and the maximum displacement is not more than 6 mm.

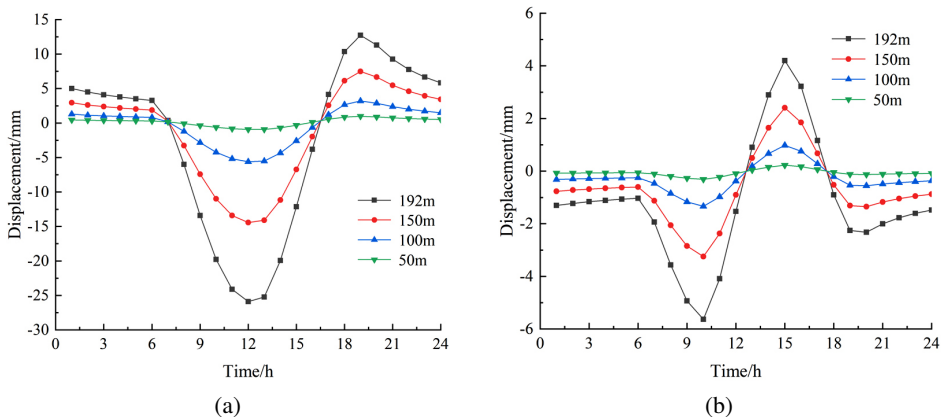


Fig. 5. The pier displacement at different heights: (a) Along the direction of the bridge, (b) The direction perpendicular to the bridge

## 4.2. The pier temperature and displacement in winter

The highest temperature is 9°C, and the lowest is 5°C. The temperature changes of the pier's outer surface in four directions were extracted and analyzed in one day. The temperature results are shown in Fig. 6. As seen from Fig. 6, the surface temperature of the piers on the southeast side began to increase at about 8 o'clock. Around 11 o'clock, the temperature on the east side appeared at an extreme value of 17°C, and then the temperature began to decrease due to the lack of solar radiation. Near 13 o'clock, the temperature on the west side gradually increased. At about 15 o'clock, the temperature on the south side appeared at an extreme value of 30°C and then began to decrease. At 17 o'clock, the temperature in the west rises to 18°C. At 21 o'clock, the sun has set, and the temperature of each surface begins to drop. At 24 o'clock, the surface temperature of the east, west, and north sides continues to decrease through convection heat transfer when the temperature of the outside atmosphere drops. The heat energy stored in the interior during the day is gradually lost, and the internal temperature is gradually stabilized. It is worth noting that the pier wall on the south side is exposed to solar radiation for the longest time, so its temperature is also higher in the whole pier, while the temperature on the north side does not change greatly in one day due to the absence of solar radiation, and is maintained around 4–6°C. In one day, the southern pier wall was subjected to solar radiation for the longest time, and its temperature variation range was 23°C.

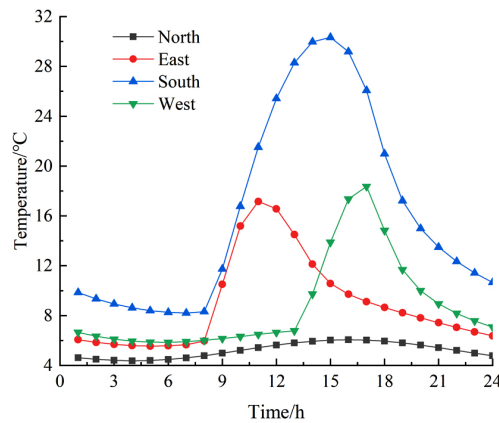


Fig. 6. Curve of pier temperature with time

The displacement changes of each section in one day were extracted and analyzed. As shown in Fig. 7, as in summer, the displacement deformation of the pier becomes more and more obvious with the increase in height. Before sunrise, the displacement curve of the pier in all directions is relatively gentle.

As can be seen from Fig. 7(a), after sunrise, the displacement of the pier body along the west direction increases, and the maximum value appears at 13 o'clock. Then, the displacement of the pier occurs in the east direction, and the displacement of the pier appears in the east direction at 18 o'clock. After sunset, the temperature of each pier wall slowly decreases and tends to be uniform, and the pier begins to recover the displacement.

As can be seen from Fig. 7(b), after sunrise, the displacement of the pier body along the north increases linearly, with a maximum value at 16 o'clock, and then the pier displaces along the south direction. After sunset, the pier displacement begins to recover slowly. Compared with the displacement in the east-west direction, it can be found that the displacement of the pier in the north-south direction is quite significant, and the displacement of the pier in the direction perpendicular to the bridge only occurs in the north direction because the north side of the pier is not affected by solar radiation.

In one day, the maximum displacement of the pier top in the direction perpendicular to the bridge is 81 mm, and the maximum displacement of the pier top along the direction of the bridge is 18 mm.

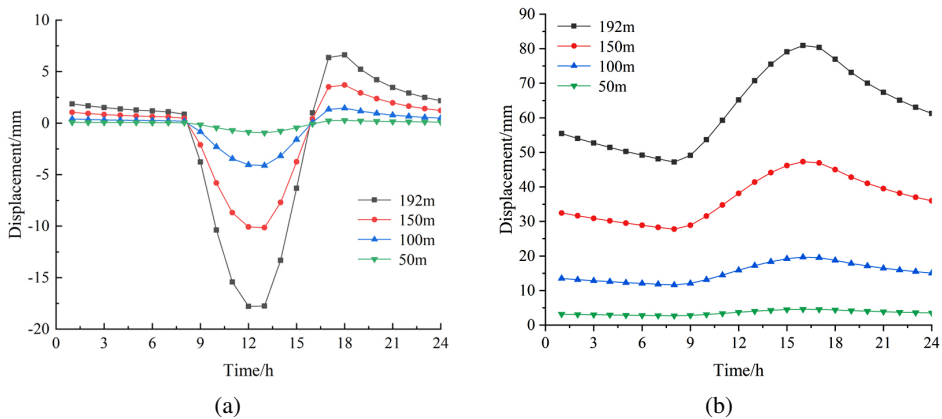


Fig. 7. The pier displacement at different heights: (a) Along the direction of the bridge, (b) The direction perpendicular to the bridge

## 5. Parametric analysis

In order to understand the influence of the change of pier cross-sectional form on the temperature and displacement of the pier body under the action of sunlight and keep the volume of the pier unchanged, the round-end and octagonal shapes are selected as the pier cross-section. The cross-sectional form of the bottom section of each pier is shown in Fig. 8, and the number 1–10 in the figure is the key point of the outer surface of the pier.

The outer surface temperature distribution curve of each cross-section pier with time in winter is shown in Fig. 9. As can be seen from Fig. 9(a), the maximum temperature of the pier with round-end cross-section occurs on the outer surface of the pier where key points 5 and 6 are located, and the maximum temperature reaches 30.4°C. The outer surface temperature of the pier where key points 1 and 10 are located controls the minimum temperature of the outer surface of the pier throughout the day.

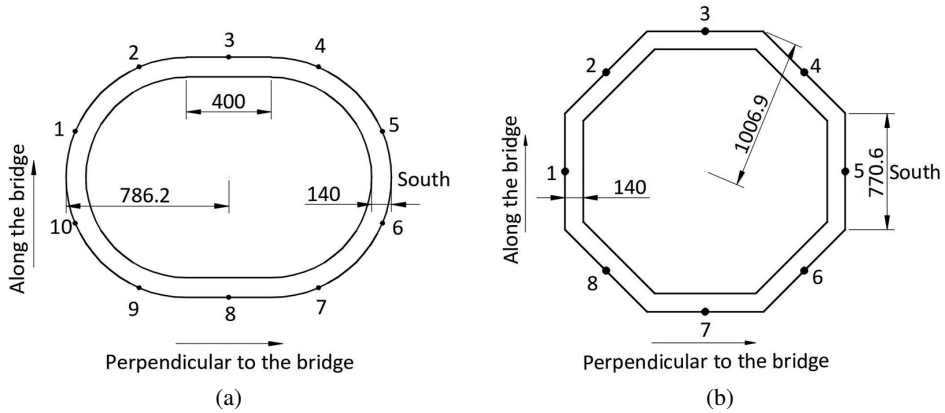


Fig. 8. Schematic diagram of the cross-section of each pier bottom (unit: cm): (a) Round-end cross-section, (b) Octagonal cross-section

As can be seen from Fig. 9(b), the maximum temperature of the octagonal cross-section pier occurs on the outer surface of the pier where key point 5 is located, and the maximum temperature reaches 30.3°C. The outer surface temperature of the pier where key point 1 is located controls the minimum temperature of the outer surface of the pier throughout the day. The surface temperature of the pier body of different cross-sections in the same direction is relatively close, and the maximum temperature of each pier wall decreases with the increase of the angle between the normal of the wall surface and the south direction in one day.

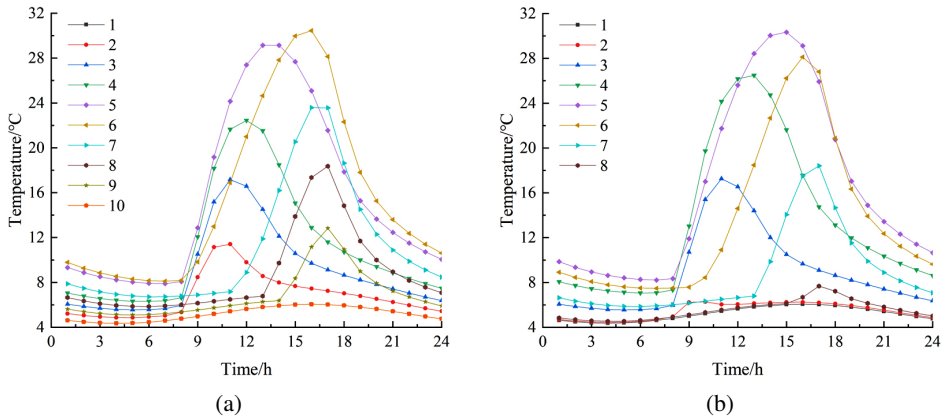


Fig. 9. Temperature distribution curves of piers with different cross-sections: (a) Round-end cross-section, (b) Octagonal cross-section

The horizontal displacement of the pier top of each cross-section on one day in winter is calculated. The variation curve of the pier top displacement is shown in Fig. 10. As can be seen from the figure, the difference between the octagonal cross-section and the rectangular cross-

section pier displacement is small, while the round-end cross-section significantly reduces the horizontal displacement of the pier top. Its essence is that the round-end cross-section increases the transverse bridge stiffness of the pier (The moment of inertia of the rectangular cross-section are  $2902.6 \text{ m}^4$  and  $2476.5 \text{ m}^4$  in the direction perpendicular to the bridge and along the direction of the bridge, respectively, and the moment of inertia of the round-end cross-section are  $3759.9 \text{ m}^4$  and  $2787.2 \text{ m}^4$ , respectively), thereby reducing the displacement of the pier.

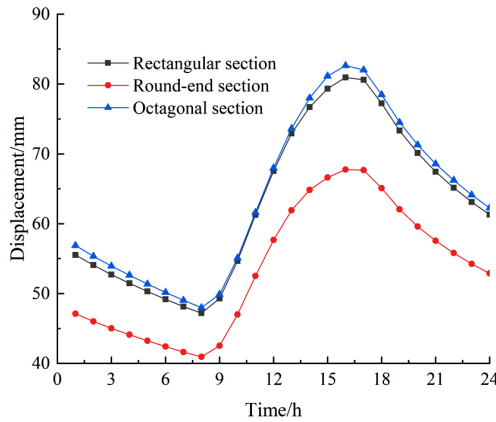


Fig. 10. The horizontal displacement of the pier top with each cross-section

## 6. Conclusions

In this paper, the temperature field and deformation of ultra-high hollow thin-walled piers under the sunlight effect is studied by using the finite element software ANSYS, and the conclusions are as follows:

1. The temperature change of the east and west pier walls is the most significant in the summer high-temperature environment. The temperature change range of the east side is  $18^{\circ}\text{C}$ , and the temperature change range of the west side is  $19^{\circ}\text{C}$ . Different from summer, the temperature change of the south pier wall is more obvious in the low temperature environment in winter, and the temperature change range is  $23^{\circ}\text{C}$ .
2. Under the action of high temperature in summer, the maximum displacement of the pier top along the direction of the bridge is 26 mm, and the maximum displacement in the direction perpendicular to the bridge is 6 mm. Under the action of low temperature in winter, the maximum displacement of the pier top along the direction of the bridge is 18 mm, and the maximum displacement in the direction perpendicular to the bridge is 81 mm. It shows that the deformation of the pier is more significant under the action of winter sunshine.
3. When the volume of the pier is kept unchanged, the displacement of the octagonal cross-section pier is close to that of the rectangular section pier, and the round-end pier can effectively reduce the displacement of the pier body caused by sunlight due to the increase of cross-sectional stiffness.

## References

- [1] H.F. Xiang, *Advanced theory of bridge structures*, 2<sup>nd</sup> ed. Beijing, China: China Communication Press, 2013.
- [2] X.F. Liu, *Temperature stress analysis of concrete structures*. Beijing, China: China Communication Press, 1991.
- [3] P.C. Jiang, “Study of temperature field in large-span steel structure under radiation-thermal-fluid coupling”, *Archives of Civil Engineering*, vol. 69, no. 1, pp. 661–674, 2023, doi: [10.24425/ace.2023.144194](https://doi.org/10.24425/ace.2023.144194).
- [4] S.C. Chen, J.Z. Yun, C.Y. Dong, W.X. Wu, and L.P. Nie, “Non-uniform temperature effect on concrete rectangular hollow bridge pier: Insights from long-term monitoring data”, *Case Studies in Construction Materials*, vol. 20, no. 4, art. no. e02801, 2023, doi: [10.1016/j.cscm.2023.e02801](https://doi.org/10.1016/j.cscm.2023.e02801).
- [5] G.L. Dai, Y. Tang, J.B. Liang, L.H. Yang, and Y.F. Chen, “Temperature monitoring of high-speed railway bridges in mountainous areas”, *Structural Engineering International*, vol. 28, no. 3, pp. 288–295, 2018, doi: [10.1080/10168664.2018.1464376](https://doi.org/10.1080/10168664.2018.1464376).
- [6] G.L. Dai, F. Wang, Y.F. Chen, H. Ge, and H.M. Rao, “Modelling of extreme uniform temperature for high-speed railway bridge piers using maximum entropy and field monitoring”, *Advances in Structural Engineering*, vol. 26, no. 2, pp. 302–315, 2023, doi: [10.1177/13694332221124618](https://doi.org/10.1177/13694332221124618).
- [7] L. An, D.J. Li, P. Yuan, and P. Chen, “An analytical algorithm for determining optimal thin-walled hollow pier configuration with sunlight temperature differences”, *Buildings*, vol. 13, no. 5, art. no. 1208, 2023, doi: [10.3390/buildings13051208](https://doi.org/10.3390/buildings13051208).
- [8] S.X. Mi, Y.Q. Wang, L.A. Li, L.J. Liao, X.J. Huo, and W. Su, “Generalized algorithm for horizontal thermal displacement at the pier top of a railway simple-supported girder bridge”, *Structures*, vol. 47, pp. 725–734, 2023, doi: [10.1016/j.istruc.2022.11.062](https://doi.org/10.1016/j.istruc.2022.11.062).
- [9] L. Zhao, “Influence of cold wave on temperature and stress fields of cylindrical concrete hollow pier”, *IOP Conference Series: Earth and Environmental Science*, vol. 267, no. 3, art. no. 032065, 2019, doi: [10.1088/1755-1315/267/3/032065](https://doi.org/10.1088/1755-1315/267/3/032065).
- [10] Y.F. Wu and Y.Y. Sun, “Influence of reinforcement on temperature and stress of hollow pier”, *Advanced Materials Research*, vol. 446–449, pp. 1319–1324, 2012, doi: [10.4028/www.scientific.net/AMR.446-449.1319](https://doi.org/10.4028/www.scientific.net/AMR.446-449.1319).
- [11] Y.H. Wang, Y.S. Zou, C.J. Li, L.Q. Xu, and S.C. Wang, “Analytical methods for temperature field and temperature stress of column pier under solar radiation”, *Mathematical Problems in Engineering*, vol. 2015, art. no. 278072, 2015, doi: [10.1155/2015/278072](https://doi.org/10.1155/2015/278072).
- [12] L. Gao, J.B. Qian, X.Z. Ding, M.Q. Guan, M.P. Liao, and Z.Q. Xu, “Experimental study for temperature variation of bridge pier in plateau area using optical frequency domain reflectometer technology”, *IEEE Sensors Journal*, vol. 23, no. 6, pp. 5810–5817, 2023, doi: [10.1109/JSEN.2023.3240314](https://doi.org/10.1109/JSEN.2023.3240314).
- [13] A.Q. Hu and C.R. Zou, “Influence of solar radiation on temperature effect of high pier of bridge in mountainous area”, *Railway Engineering*, vol. 61, pp. 23–27, 2021.
- [14] Q. Yuan, W.T. Liu, H.M. Rao, H. Xie, and H. Zhao, “Effect of reflective coatings on temperature effect of RC round-ended pier of high-speed rail bridge under thermal radiation”, *Journal of The China Railway Society*, vol. 41, no. 7, pp. 95–101, 2019.
- [15] B. Fu, “Temperature field calculation and influencing factors analysis for concrete hollow piers under solar radiation”, *Journal of Information and Computational Science*, vol. 10, no. 4, pp. 1007–1016, 2013, doi: [10.12733/jics20101477](https://doi.org/10.12733/jics20101477).
- [16] O. Kordun, “The influence of solar radiation on temperature increment of sheet steel structures”, *Archives of Civil Engineering*, vol. 61, no. 1, pp. 89–102, 2015, doi: [10.1515/ace-2015-0006](https://doi.org/10.1515/ace-2015-0006).
- [17] H. Wang, “Study on Solar Radiation Temperature Field and Effect of Hollow Concrete Pier”, MSc. thesis, Chongqing University, Chongqing, China, 2012.
- [18] J.Z. Mao, “Study on Temperature Field and Effects of Hollow High Pier”, MSc. thesis, Beijing Jiaotong University, Beijing, China, 2016.